analytical chemistry

pubs.acs.org/ac
Article

Digital Lasing Biochip for Tumor-Derived Exosome Analysis

Tian Zhou, Guocheng Fang,* Ziyihui Wang, Zhen Qiao, Ningyuan Nie, Bowen Fu, Po-Hao Tseng, Xiyu Sun, and Yu-Cheng Chen*

Cite This: *Anal. Chem.* 2025, 97, 5605−5611
Read Online

ABSTRACT: Digital microfluidics represents an emerging versatile platform that offers numerous advantages in biomolecule detection. However, conventional probes often lack high-intensity and high-sensitivity signals, making it challenging for precise and automatic analysis. Recently, optical microresonators stand as a prominent high-sensitivity detection in the biological field. Here we introduce whispering gallery mode (WGM) microlasers into the microwell array, forming a digital lasing detection system. The lasing signal makes it highly sensitive, which amplifies the subtle changes via the strong interactions of light and matter. The microfluidic droplet technique further allowed microlasers with uniform laser thresholds and high-throughput fabrication. We utilized this tool for the analysis of exosomes derived from tumor spheroids. We believe that this digital optofluidic system could serve as a promising tool in diverse biomolecule assays and various biomedical applications.

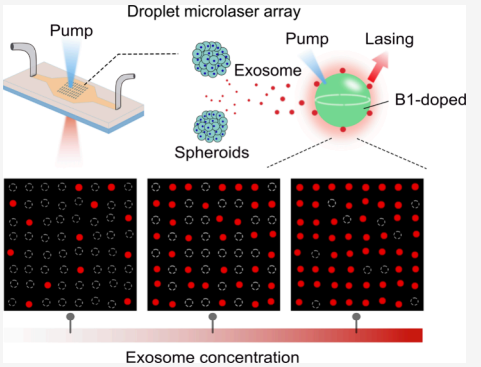

INTRODUCTION

Exosomes contain various kinds of cellular-related materials, such as proteins, lipids, and RNA (mRNA and miRNA), which have now been recognized as vital mediators of intercellular communication, cell maintenance, and tumor progression. They play a pivotal role in modulating immune responses, serving as carriers of antigen-presenting vesicles.[1−5] For instance, within the nervous system, exosomes facilitate myelination, neurogenesis, and neuronal viability, thus actively participating in tissue repair and regeneration processes.[6−8] Recently, exosomes are garnering interest for their potential as biomarkers in liquid biopsy. By isolating and analyzing exosomes from bodily fluids, it helps to gain insights into various disease processes, including tumors, neurodegenerative disorders, and inflammatory conditions. For example, exosomes isolated from urine have shown promise in reflecting acute kidney injury.[9−11] Additionally, exosomes offer a more comprehensive and dynamic view of disease biomarkers compared with traditional tissue biopsies, which provide only a snapshot of the disease at a specific time point.

Microfluidics have risen as a prevalent and effective methodology for analyzing exosomes, leveraging a combination of chemical, biological, and optical characteristics.[12−16] The realm of microfluidics has garnered substantial attention and acclaim due to its inherent advantages in biochemical analysis including minimal sample volumes, amplified reaction speed, and multiplex detecting. In the sphere of exosome detection, the integration of optofluidics has emerged as a significant and promising approach. This convergence, uniting the prowess of optics with microfluidics, presents remarkable advantages, offering heightened sensitivity in optical signaling and exceptionally rapid detection time.[17−20] For instance, the fluorescence-based digital microfluidics has enhanced the analytical capabilities significantly, including high-throughput, real-time monitoring, and precise quantification. However, the minute dimensions of exosomes inherently limit the signals they emit, posing challenges in their observation and rendering them susceptible to interference within the complex biological fluid milieu. Several advanced techniques have been developed to enable exosome detection with high sensitivity. Raghu et al. introduced a nanoplasmonic pillar array that facilitates real-time single-exosome detection by monitoring spectral changes.[21] Su et al. reported a real-time, label-free spectroscopic method for detecting tumor-derived exosomes at the single-molecule level, achieving a detection precision better than 10 am (attometers).[22] This approach holds significant promise for minimally invasive tumor diagnostics. Im et al. developed the nanoplasmonic exosome (nPLEX) assay, which leverages surface plasmon resonance (SPR) to enable single-exosome detection by analyzing the resonant spectrum.[23] Furthermore, this technique can be integrated with optical systems to create portable diagnostic devices. While these advancements have demonstrated impressive sensitivity, there remains a critical need for complementary tools, particularly imaging-based techniques, to further enhance signal amplifica-

Received: November 15, 2024
Revised: February 3, 2025
Accepted: February 17, 2025
Published: March 5, 2025

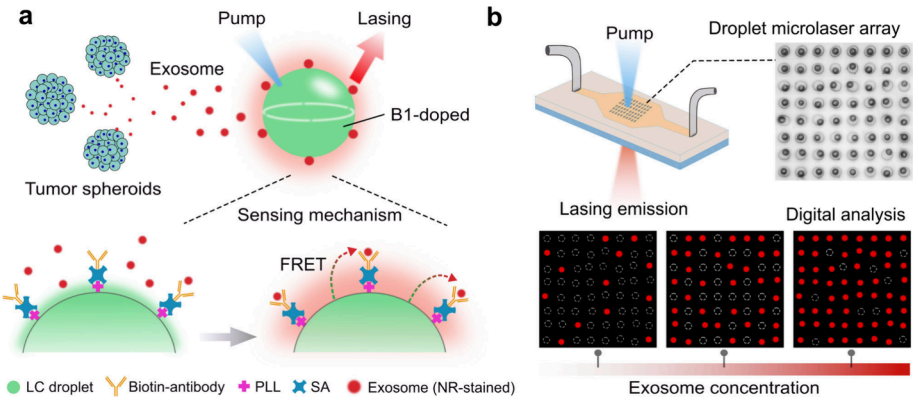

Figure 1. Concept of the digital lasing biochip for exosome analysis. (a) Illustrations of a lasing microdroplet designed for sensing exosomes (top) and the laser response to exosomes via fluorescence resonance energy transfer (FRET) (bottom). When the NR-stained exosomes were captured by the LC droplets, FRET occurred at the droplet interface, leading to a reduced threshold of laser emission at red wavelength. (b) Schematic concept of the digital exosome detection system and bright-field image of the microdroplet array (top). Lasing emission images showed digital microlaser array responsive to various concentrations of exosomes (bottom).

tion and ensure stable output in complex biological environments.

Laser emissions, which are intensified through optical resonators, offer distinct advantages such as enhanced coherence, brightness, line width, and signal-to-noise ratio.[24−31] The unique laser spectrum and threshold offered by microlasers have proven pivotal in numerous investigations, showcasing their versatility for cellular and tissue applications.[32−35] Noteworthy are laser-emitting particles utilizing whispering gallery modes (WGM), renowned for their profound light−matter interactions along the cavity interface. Their exceptional sensitivity to changes in the surrounding environment positions them as ideal candidates for precise and nuanced digital sensing capabilities at the single-molecule level.[36,37]

Given the rapid development of microlaser-based biosensors, most of the reported sensors require precise spectral analysis through optical spectrometer. To overcome the bottleneck, here in this study, we proposed a digital microlaser array for rapid quantification of laser emissions upon capturing specific antibodies. As shown in Figure 1, we developed an integrated optofluidic system to detect extracellular vesicles, expressing a multifaceted array of digital detection outcomes. The establishment of the sensing functionality relied on surface-modified microdroplets introduced into a specialized microwell array. Harnessing the principles of resonance energy transfer at the cavity interface, the emissions detected within the cavity underwent a fascinating transition from the green band (donor molecule) to the red band (acceptor molecule) upon successful binding events (Figure 1a).[38−40] This detection mechanism capitalizes on the overlap between the emission band of microlasers doped with Bodipy 1 (B1)-droplets and the absorption band of Nile Red (NR) vesicles (Supporting Information Figure S1). By introducing the microdroplet lasers into the microwell array and analyzing the laser emissions via cameras, a digital platform was setup for precise quantification (Figure 1b). We utilized this tool for tumor-spheroid-derived exosome analysis on the chip, which further expressed good specificity to various types of exosomes. Compared to fluorescence digital analysis, the lasing digital method provides a higher level of granularity and accuracy in detection.

MATERIALS AND METHODS

Materials. 4′-Pentyl-4-biphenylcarbonitrile, a nematic liquid crystal (5CB), was obtained from Sigma-Aldrich (no. 328510). Poly(vinyl alcohol) (PVA) was sourced from Sigma-Aldrich (no. P8136). The green dye Bodipy-1 and Nile Red were acquired from Sigma-Aldrich (nos. 793728 and 72485, respectively). Surface-modified microcavities were prepared using poly-L-lysine solution (Sigma-Aldrich, no. P4832), streptavidin (SA; Sigma-Aldrich, no. S4762), and bovine serum albumin solution (BSA; Sigma-Aldrich, no. A8412). The biotin-linked antibodies utilized included Anti-CD9 (Thermo Fisher, no. 13-0098-82), anti-CD63 (Biolegend, no. 353018), and anti-CD81 (Biolegend, no. 349514). Total exosome isolation reagent (for cell culture media) was procured from Thermo Fisher (no. 4478359). SU-8 2010 and its developer were purchased from Kayaku Advanced Materials (Westborough, MA, USA). The silicone elastomer Sylgard 184 (Dow Corning, USA) was used as a two-component kit comprising a prepolymer and a curing agent with a default mixing weight ratio of 10:1.

Fabrication of Microfluidic Chip and Microwell Array. Microfluidic devices were fabricated by using photolithography. A 4 inch silicon wafer was first spin-coated with SU-8 2010 to create a layer about 25 μm thick. Following a soft bake, the wafer was exposed to UV light to form a pattern at 170 mJ/cm^2; then it received a postexposure bake before development.The molds were fabricated via an ultraviolet maskless lithography machine [TuoTuo Technology (Suzhou) Co., Ltd.].

For molding, polydimethylsiloxane (PDMS) was prepared. A plasma surface treatment machine (Diener Electronic, Ebhausen, Germany) activated the PDMS and the glass surfaces. The PDMS was then pressed onto a glass slide. Finally, the microchannels were made hydrophilic by flushing with a 1% PVA solution in deionized water.

Microfluidic Droplet Generation and Surface Modification. To produce dye-doped liquid crystal (LC) microbeads, 3.3 mg of B1 was added to 500 μL of LC to form the dispersed phase. This was then combined with a continuous phase consisting of a 2% PVA solution (PVA dissolved in deionized water). Pressure pumps were used to precisely control the flow of liquids within the microbead generation chip. The flow rates were set at 0.2 μL/min for the dispersed

https://doi.org/10.1021/acs.analchem.4c06172
Anal. Chem. 2025, 97, 5605−5611

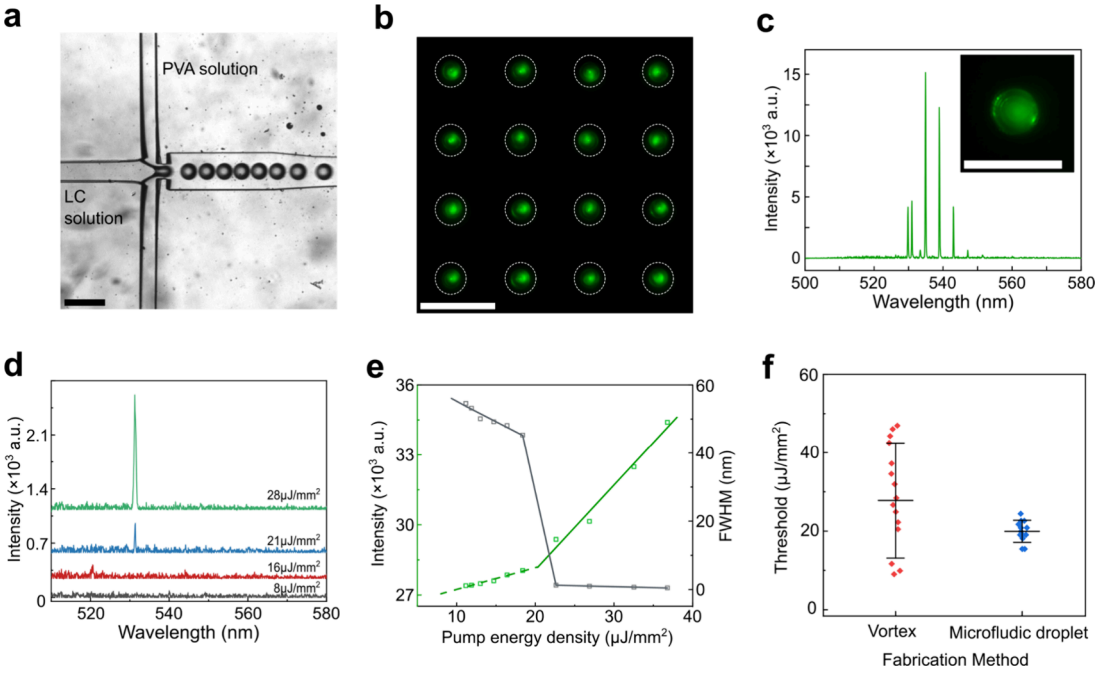

Figure 2. Optical characterization of B1-doped droplet microlasers. (a) Microfluidic device for LC microlaser fabrication. (b) Laser emission images of the B1-doped LC microdroplets in a microwell array. The microwells are labeled by white dashed circles. (c) Typical spectrum of laser emission of a B1-doped LC droplet. The spectrum showed ultranarrow peaks at the wavelength range of 520−550 nm. Inset is the image of a single lasing droplet. (d) Laser spectra at various pump densities. (e) Laser threshold plot and fwhm plot of the droplet microlasers. (f) Laser threshold distribution of microdroplets fabricated by the vortex method and microfluidic droplet technique. Scale bar: 40 μm.

phase and 1 μL/min for the continuous phase, resulting in the formation of uniform dye-doped LC microbeads, which were subsequently collected through a tube.

Following this, a 2.5 mL poly-L-lysine (PLL) solution was introduced into the tube to functionalize the cavities, leveraging their positively charged property. After an incubation period of 40 min, a 200 mg/mL SA solution was utilized to coat the LC droplets for an additional 40 min. To prevent nonspecific bindings on the surface, a 1 mg/mL BSA application was added. Each step involved washing the microcavities with a PBS solution and subsequent centrifugation to remove excess PLL, SA, and BSA molecules from the surrounding environment. Finally, various biotin-linked antibodies were introduced to bind with the microcavities, facilitating the attraction of exosomes and their corresponding protein biomarkers (antigens).

Collection of Exosomes from Tumor Cells and Spheroids. The cultivation of tumor spheroids and extraction of exosomes secreted from cells were conducted as described in previous reports.[41] A549 cancer cells, sourced from ATCC, were grown in RPMI1640 medium enriched with 10% fetal bovine serum (FBS) and 100 units/mL of penicillin/streptomycin. Cells were cultured to 70−80% confluence in a Petri dish within a humidified incubator at 37 °C and 5% CO_2, after which they underwent passage. The cells underwent 3−4 passages before use. Spheroids were produced using the agarose microwell technique.[42] Prior to cell loading, the agarose chips were immersed in PBS for a minimum of 1 day. Following a 3 min treatment with trypsin−EDTA solution and a 5 min centrifugation at 500*g*, the supernatant was discarded, and the cells were resuspended in 1 mL of fresh medium to achieve a concentration of 1×10^6 to 1×10^7 cells/mL. The cells were then seeded onto a microwell chip and incubated, resulting in the formation of spheroids within 1−2 days. The medium was refreshed bi-daily, and the conditioned medium was harvested for exosome detection.

Two methods were employed for staining and subsequent sensing: (1) Direct sensing within the cellular environment was achieved by staining exosomes with 3 nM NR added to the cell medium. (2) For exosome separation and sensing, exosomes were enriched using the Invitrogen Total Exosome Isolation kit from the cell medium. A NR solution was then added to the isolated exosomes and incubated for 2 min. Subsequently, the samples underwent centrifugation twice at 10000*g* for 1 h at 4 °C to eliminate excess Nile Red molecules, after which the NR-labeled exosomes were resuspended in a PBS solution.

Optical System Setup. To activate the modified resonators within the microwell testing array, a pulsed laser (EKSPLA NT230) with a pulse duration of 5 ns (repetition rate, 50 Hz) was utilized alongside an upright microscopic system (Nikon Ti2). The pump wavelength used was 480 nm with a tunable pump laser energy set at 60 and 70 μJ/mm^2 during the exosome detection stage. Emission light was collected and directed into a charge-coupled device (CCD) camera and imaging spectrometer (Andor Kymera 328i/Newton 970 EMCCD) for analysis.

RESULTS AND DISCUSSION

Optical Characterization of Droplet Microlaser. To ensure reliable detection outcomes, it is essential to obtain microlaser sensors with consistent dimensions and quality factors. We used a microfluidic droplet technique to generate LC microlasers (Figure 2a), designing them to be approximately 20 μm in diameter. This size supports both a high *Q*-factor of ~3.4×10^4 and ease of manipulation. The resulting LC microlasers exhibited a remarkably uniform size, with diameters of 21 ± 2 μm, compared to those produced by the vortex emulsion (Figure S3). LC microlasers can be stored in a

https://doi.org/10.1021/acs.analchem.4c06172
Anal. Chem. 2025, 97, 5605−5611

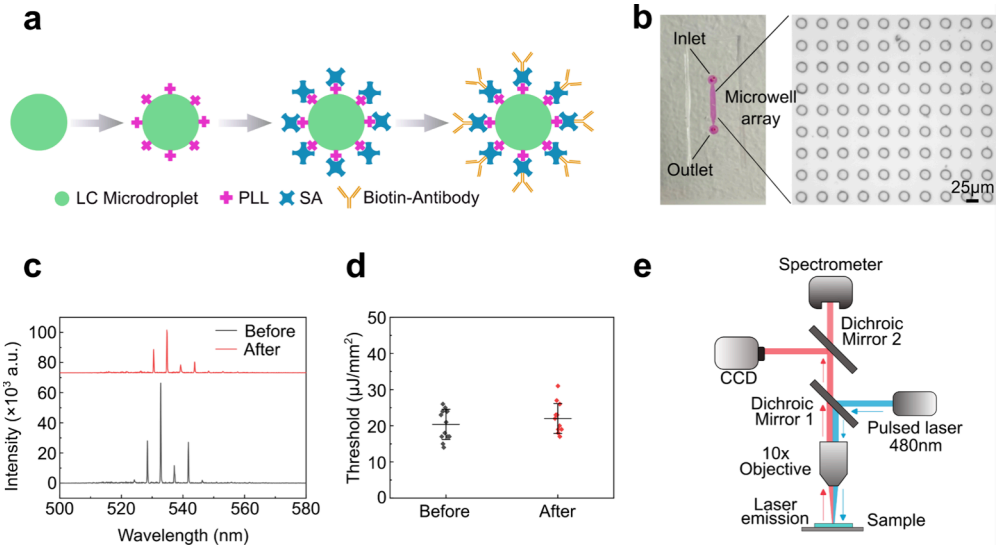

Figure 3. LC droplet surface modification and setup of the detection system. (a) Illustration of the surface modification of the LC microdroplets. (b) Image of the microwell array for exosome detection. (c) Spectra of laser emissions of LC microdroplets before and after the surface modification. (d) Threshold distribution of microdroplets before and after the surface modification. (e) Illustration of the optical setup for laser excitation and detection.

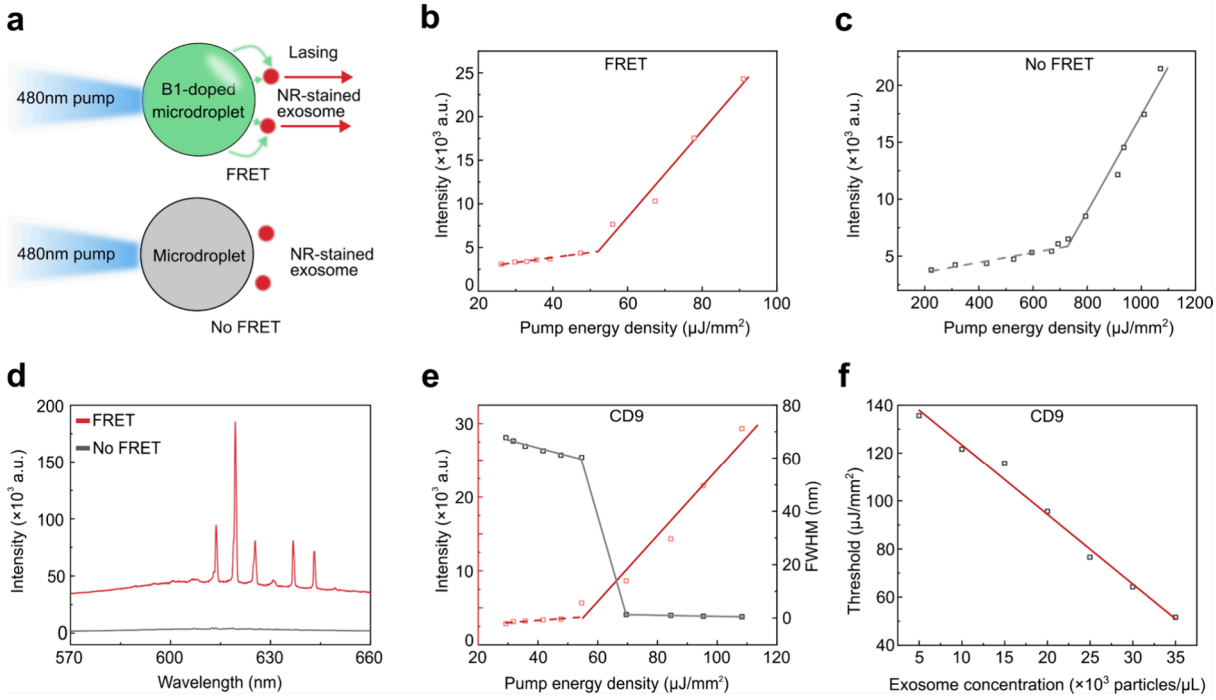

Figure 4. FRET lasing mechanism after capturing the NR-stained exosomes. (a) Comparation of the lasing energy transfer between droplets with and without B1 doping. When the NR-stained exosomes bind to the droplets with high-concentration B1 inside, FRET occurs between the droplet surface and the NR molecules on the exosomes. (b, c) Spectrally integrated laser output against the pump energy density. The dashed line indicates the linear fit for pump energy density below the threshold, and a solid line represents the linear fit for energy density surpassing the threshold. The lasing threshold was ~52 μJ/mm^2 for FRET droplets and 710 μJ/mm^2 for non-FRET droplets. (d) Lasing spectra after exosomes binding with FRET or non-FRET mechanism. The pumping energy was fixed at 60 μJ/mm^2 under both conditions. (e) Laser threshold and fwhm of the FRET lasing emission of the modified droplets specifically bonded with exosomes. The droplets were surface-modified with CD9 antibody and exhibited specific binding with the exosomes. (f) Correlation between the threshold of CD9 antibody-modified LC microlasers and the concentration of the exosomes.

2% PVA solution for several months. We further loaded the LC microlasers into a microwell array for optical characterization under a 480 nm pulsed pump. The LC microlasers demonstrated robust WGM lasing at 520−550 nm (Figure 2b,c) with ultranarrow laser peaks. The inset shows an image of WGM lasing, specifically along the droplet's outer boundary (Figure 2c). Under varying pump intensities, the LC microlasers exhibited a clear lasing threshold, generally around 21 μJ/mm^2, with a full width at half-maximum (fwhm) of up to 0.2 nm (Figures 2d,e). This droplet uniformity is essential for

https://doi.org/10.1021/acs.analchem.4c06172
Anal. Chem. 2025, 97, 5605−5611

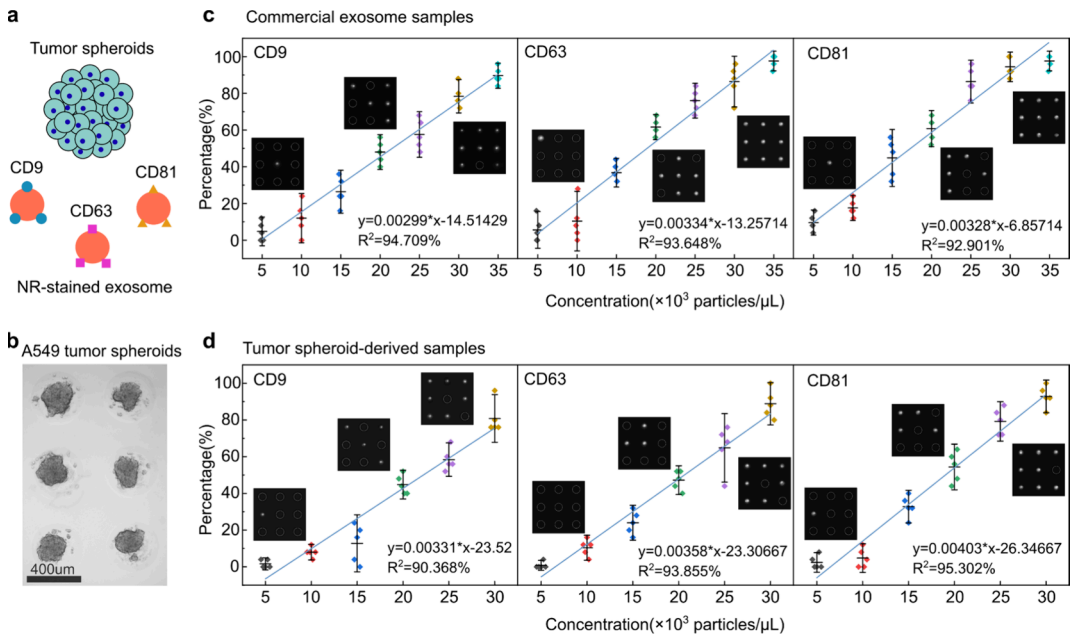

Figure 5. Detection of exosomes derived from tumor spheroids. (a) Illustration of A549 tumor spheroids and exosomes with different tetraspanins (CD9, CD63, and CD81). (b) Bright-field image of A549 tumor spheroids cultured in agarose microwells. (c) Correlations between the concentration of the commercial exosome samples and the percentage of lasing droplets. Inset: droplet laser images were captured by CCD at low, medium, and high concentrations of the exosomes. The droplets that cannot generate laser emission are marked with red dashed circles. (d) Analogous correlations under identical experimental conditions, where the samples derived from A549 tumor spheroids. Droplet laser images were captured by CCD under low, medium, and high concentrations of the exosomes. The droplets that cannot generate laser emission are marked with white dashed circles. All of the testing were conducted in a 10 × 10 microwell area.

accurate digital lasing analysis. Statistical testing of droplet thresholds revealed a narrow distribution (15−25 μJ/mm^2) for microfluidic droplets, in contrast to the broader range (5−50 μJ/mm^2) observed in droplets generated by vortex emulsion (Figure 2f).

Surface Modification of Droplet Microlasers. To enable the capture of specific tumor-derived exosomes, we modified the microlaser surfaces with specific antibodies (Figure 3a). Details of the procedure are available in Materials and Methods. We designed a PDMS microfluidic chip with a microwell array to secure the microlasers, enhancing exosome capture and facilitating digital analysis (Figure 3b). The detection area, approximately 1 cm × 3 cm, contains over 15000 microwells with the microwell diameter of around 25 μm. After surface modification, the microlasers exhibited a wavelength shift of 2−3 nm, which was attributed to changes in the surface refractive index (Figure 3c). The average lasing threshold increased slightly, from 20 to 23 μJ/mm^2 (Figure 3d), while maintaining a narrow threshold distribution, comparable to their performance prior to modification. Digital analysis is conducted via an optical system with scanning capability (Figure 3e). The pump light was fixed at 480 nm to excite B1.

FRET Lasing Mechanism for Exosome Analysis. To enhance the detection sensitivity, we designed a FRET system with B1 molecules (donor) in the microlasers and NR molecules (acceptor) on the exosomes. When NR-stained exosomes are captured by the microlasers, NR molecules can be excited by emission from the B1 donors, generating laser emission not only at the green wavelength but also at the red wavelength. In our analysis, we focused on lasing at the red wavelength using the FRET mechanism.

To evaluate FRET lasing efficiency, we compared lasing dynamics in two configurations: one group of droplets containing B1 donors and another group without. Both droplet types were excited by a 480 nm pulsed laser under identical conditions (Figure 4a). Results showed that, at a fixed exosome concentration, the FRET group exhibited a significantly reduced laser threshold, averaging ∼52 μJ/mm^2, compared to ∼710 μJ/mm^2 in the non-FRET group (Figure 4b,c), a 92.3% reduction in threshold. As a result, FRET-enabled droplets produced a distinct red laser emission (Figure 4d).

For selective exosome detection, we surface-modified the microlasers with antibodies against CD9, CD63, and CD81, common exosome markers in cancer cells that play roles in cancer cell proliferation, invasion, and metastasis. After a 20 min incubation with the exosome sample, we measured the lasing threshold and fwhm of each droplet group (Figure 4e, Figure S4). The commercial exosome sample had a concentration exceeding 40000 particles/μL, ensuring sufficient exosome capture to demonstrate FRET-based lasing performance. Results indicated that all droplets exhibited a threshold range of 40−60 μJ/mm^2. Specifically, droplets targeting CD81 exosomes required a higher pump energy density, while those targeting CD9 needed a lower energy density. fwhm performance was generally consistent across groups, although differences in biomarkers led to variations in lasing emission signals.

As exosome concentration increased, the microlaser threshold decreased, allowing FRET lasing emission to occur more readily under a fixed pump energy (Figure 4f, Figure S5). In practical applications, a higher proportion of microlasers producing red lasing signals indicated a higher exosome concentration.

https://doi.org/10.1021/acs.analchem.4c06172
Anal. Chem. 2025, 97, 5605−5611

Detection of Tumor Spheroid-Derived Exosomes. Tumor spheroids are physiologically 3D models relevant to native tumors that have been widely used in disease modeling and drug screening.[42−44] Exosomes-derived from the tumor spheroids gives an insight into intracellular communications and tumor development.[45−48] Here we utilized the developed platform to detect the exosomes derived from A549 lung tumor spheroids (Figure 5a,b). The spheroids were cultured in the microwell array and had an average diameter of ∼300 μm.

We first utilized the commercial exosome samples for the assessment of the microlaser's sensitivity (Figure 5c). Leveraging prior investigations, we set the pumping energy density slightly above the thresholds (70 μJ/mm^2 for CD9, 60 μJ/mm^2 for CD63, and 70 μJ/mm^2 for CD81). All three microlasers exhibited an expansive detection range spanning from 5000 to 35000 particles/μL, displaying commendably high linear correlations. Noteworthy, the CD81 group showcased earlier saturation when exosome concentration was above 25000 particles/μL, indicating a potential reduced sensitivity at high exosome concentration compared with the other two groups. To fortify the result credibility, we conducted experiments under identical conditions for five cycles across each concentration level and microsensor group. The outcomes demonstrated a confined distribution range, implying an acceptable consistency.

We then detected the samples derived from the A549 tumor spheroid (Figure S6). The detection outcomes of the tumor spheroid-derived samples displayed a narrower range (5000 to 30000 particles/μL) compared to the control group when using the same experimental conditions yet maintaining a notable linear correlation (Figure 5d). The consistent outcomes observed between the experimental group and the control group affirm not only the reliability but also the robust functionality of these microlasers.

CONCLUSION

In this study, we developed a digital lasing device that can achieve the digital analysis for exosomes in a fluidic biological environment. The strong light−matter interactions of the droplet lasers amplified subtle changes in the molecular level. In addition, leveraging the FRET mechanism at the droplet cavity interface, the laser emissions were more sensitive to the exosome concentrations. The fabrication of LC droplets through the microfluidics can ensure uniform laser characteristics (e.g., threshold, emission wavelength, etc.) and the credibility of digital analysis.

The versatility of microlasers can also extend beyond exosome detection, respectively, including mRNA, circulating DNA, and small metabolites. The emission wavelength of microlasers can be flexibly designed by altering the gain material in LC droplets, thereby enabling multiplexing detection due to the narrow line width of the laser emissions. This integrated system can serve as an available tool for both fundamental biological science and practical applications, including medical diagnostics and personalized healthcare.

ASSOCIATED CONTENT

Supporting Information

The Supporting Information is available free of charge at https://pubs.acs.org/doi/10.1021/acs.analchem.4c06172.

(Figure S1) Organic dyes' normalized absorption and emission spectra; (Figure S2) microfluidic fabrication device design; (Figure S3) droplets characteristics; (Figure S4) lasing threshold and full width at half-maxima; (Figure S5) exosomes concentration correlations with LC microsensors thresholds; (Figure S6) lasing spectral microlaser responses (PDF)

AUTHOR INFORMATION

Corresponding Authors

Guocheng Fang − *School of Electrical and Electronics Engineering, Nanyang Technological University, Singapore 639798, Singapore*; Email: guocheng.fang@ntu.edu.sg

Yu-Cheng Chen − *School of Electrical and Electronics Engineering, Nanyang Technological University, Singapore 639798, Singapore*; orcid.org/0000-0002-0008-5601; Email: yucchen@ntu.edu.sg

Authors

Tian Zhou − *School of Electrical and Electronics Engineering, Nanyang Technological University, Singapore 639798, Singapore*

Ziyihui Wang − *School of Precision Instrument and Optoelectronics Engineering, Tianjin University, Tianjin 300072, China*; orcid.org/0000-0002-8261-8298

Zhen Qiao − *School of Optical-Electrical and Computer Engineering, University of Shanghai for Science and Technology, Shanghai 200093, China*

Ningyuan Nie − *School of Electrical and Electronics Engineering, Nanyang Technological University, Singapore 639798, Singapore*

Bowen Fu − *School of Electrical and Electronics Engineering, Nanyang Technological University, Singapore 639798, Singapore*

Po-Hao Tseng − *School of Electrical and Electronics Engineering, Nanyang Technological University, Singapore 639798, Singapore*

Xiyu Sun − *School of Electrical and Electronics Engineering, Nanyang Technological University, Singapore 639798, Singapore*

Complete contact information is available at: https://pubs.acs.org/10.1021/acs.analchem.4c06172

Author Contributions

T.Z., Z.W., G.F., and Y.-C.C. conceived and designed the experiments. T.Z., G.F., and N.N. performed the optical experiments. G.F. and P.-H.T. conducted the cellular preparation and experiments. T.Z., B.F, X.S., and G.F. designed and fabricated the microfluidic devices. T.Z., G.F., and Y.-C.C. analyzed the data. Z.W., Z.Q., X.S., and G.F. provided useful advice and supporting resources. T.Z. and G.F. wrote the manuscript. Y.-C.C. supervised the whole research.

Notes

The authors declare no competing financial interest.

ACKNOWLEDGMENTS

This work was supported by an A*STAR MTC IRG-Grant (M21K2c0106, Singapore).

REFERENCES

(1) Essola, J. M.; Zhang, M.; Yang, H.; Li, F.; Xia, B.; Mavoungou, J. F.; Hussain, A.; Huang, Y. *Bioact. Mater.* **2024**, *32*, 124−146.

(2) Shenoda, B. B.; Ajit, S. K. *Clin. Med. Insights:: Pathol.* **2016**, *9s1*, 1−8.

(3) Lyu, C.; Sun, H.; Sun, Z.; Liu, Y.; Wang, Q. *Cell Death Dis.* **2024**, *15* (2), 106.
(4) Wu, R.; Gao, W.; Yao, K.; Ge, J. *Front. Immunol.* **2019**, *10*, 648.
(5) Zhou, X.; Xie, F.; Wang, L.; Zhang, L.; Zhang, S.; Fang, M.; Zhou, F. *Cell. Mol. Immunol.* **2020**, *17* (4), 323−334.
(6) Zhong, L.; Wang, J.; Wang, P.; Liu, X.; Liu, P.; Cheng, X.; Cao, L.; Wu, H.; Chen, J.; Zhou, L. *Stem Cell Res. Ther.* **2023**, *14* (1), 198.
(7) Wang, Y.-y.; Cheng, J.; Liu, Y.-d.; Wang, Y.-p.; Yang, Q.-w.; Zhou, N. *Biomed. Pharmacother.* **2023**, *169*, No. 115920.
(8) Pishavar, E.; Trentini, M.; Zanotti, F.; Camponogara, F.; Tiengo, E.; Zanolla, I.; Bonora, M.; Zavan, B. *ACS Nanosci. Au* **2022**, *2* (4), 284−296.
(9) Doyle, L. M.; Wang, M. Z. *Cells* **2019**, *8* (7), 727.
(10) Oh, S.; Kwon, S. H. *Int. J. Mol. Sci.* **2021**, *22* (16), 8913.
(11) Sun, I. O.; Lerman, L. O. *Diagnostics* **2020**, *10* (5), 311.
(12) Altıntaş, Ö.; Saylan, Y. *Anal. Chem.* **2023**, *95* (44), 16029−16048.
(13) Chen, C.; Skog, J.; Hsu, C.-H.; Lessard, R. T.; Balaj, L.; Wurdinger, T.; Carter, B. S.; Breakefield, X. O.; Toner, M.; Irimia, D. *Lab Chip* **2010**, *10* (4), 505−511.
(14) Liga, A.; Vliegenthart, A. D. B.; Oosthuyzen, W.; Dear, J. W.; Kersaudy-Kerhoas, M. *Lab Chip* **2015**, *15* (11), 2388−2394.
(15) Le, M.-C. N.; Fan, Z. H. *Biomed. Mater.* **2021**, *16* (2), No. 022005.
(16) Su, W.; Li, H.; Chen, W.; Qin, J. *TrAC, Trends Anal. Chem.* **2019**, *118*, 686−698.
(17) Kanwar, S. S.; Dunlay, C. J.; Simeone, D. M.; Nagrath, S. *Lab Chip* **2014**, *14* (11), 1891−1900.
(18) Dias, T.; Figueiras, R.; Vagueiro, S.; Domingues, R.; Hung, Y.-H.; Persia, E.; Arsène, P. An electro-optical bead-nanochip technology for the ultrasensitive and multi-dimensional detection of small extracellular vesicles and their markers. *bioRxiv Preprint*, 2022, 2022.2004.2011.487936. https://doi.org/10.1101/2022.04.11.487936.
(19) Vázquez-Guardado, A.; Barkam, S.; Peppler, M.; Biswas, A.; Dennis, W.; Das, S.; Seal, S.; Chanda, D. *Nano Lett.* **2019**, *19* (1), 449−454.
(20) Liu, Y.; Zhang, Y.; Wang, C.; Wang, Y.; Zhang, K.; Yang, X.; Peng, G.-D.; Liu, S.; Wang, Z.; Rao, Y.-J.; Gong, Y. *Sens. Actuators, B* **2024**, *403*, No. 135198.
(21) Raghu, D.; Christodoulides, J. A.; Christophersen, M.; Liu, J. L.; Anderson, G. P.; Robitaille, M.; Byers, J. M.; Raphael, M. P. *PLoS One* **2018**, *13* (8), No. e0202773.
(22) Su, J. *ACS Photonics* **2015**, *2* (9), 1241−1245.
(23) Im, H.; Shao, H.; Park, Y. I.; Peterson, V. M.; Castro, C. M.; Weissleder, R.; Lee, H. *Nat. Biotechnol.* **2014**, *32* (5), 490−495.
(24) Zhao, Y.; Lin, C.; Wu, P.; Chen, X.; Zhao, Y.; Li, Y.; Chen, L.; Nilsson, M.; Ke, R. *ACS Sens.* **2020**, *5* (10), 3031−3036.
(25) Zhao, N.-n.; Li, F.-z.; Zhang, X.; Liu, M.; Cao, H.; Zhang, C.-y. *Anal. Chem.* **2023**, *95* (22), 8728−8734.
(26) Zhou, J.; Wu, Y.; Lee, S.-K.; Fan, R. *Lab Chip* **2012**, *12* (23), 5025−5033.
(27) Zhang, Y.; Zhang, C.; Fan, Y.; Liu, Z.; Hu, F.; Zhao, Y. S. *ACS Appl. Mater. Interfaces* **2021**, *13* (16), 19187−19192.
(28) Guo, J.; Haehnle, B.; Hoenders, D.; Creusen, G.; Jiao, D.; Kuehne, A. J. C.; Walther, A. *Adv. Mater.* **2020**, *32* (29), No. 2002332.
(29) Xu, F. F.; Li, Y. J.; Lv, Y.; Dong, H.; Lin, X.; Wang, K.; Yao, J.; Zhao, Y. S. *CCS Chem.* **2020**, *2* (6), 369−375.
(30) Fang, G.; Ho, B. X.; Xu, H.; Gong, C.; Qiao, Z.; Liao, Y.; Zhu, S.; Lu, H.; Nie, N.; Zhou, T.; et al. *ACS Nano* **2024**, *18* (38), 26338−26349.
(31) Fang, G.; Qiao, Z.; Huang, L.; Zhu, H.; Xie, J.; Zhou, T.; Xiong, Z.; Su, I. H.; Jin, D.; Chen, Y.-C. *Nat. Commun.* **2024**, *15* (1), 7332.
(32) Demina, P. A.; Sindeeva, O. A.; Abramova, A. M.; Saveleva, M. S.; Sukhorukov, G. B.; Goryacheva, I. Y. *J. Biophotonics* **2023**, *16* (6), No. e202200379.
(33) Gather, M. C.; Yun, S. H. *Nat. Photonics* **2011**, *5* (7), 406−410.
(34) Tang, S.-J.; Dannenberg, P. H.; Liapis, A. C.; Martino, N.; Zhuo, Y.; Xiao, Y.-F.; Yun, S.-H. *Light: Sci. Appl.* **2021**, *10* (1), 23.
(35) Chen, Y.-C.; Chen, Q.; Zhang, T.; Wang, W.; Fan, X. *Lab Chip* **2017**, *17* (3), 538−548.
(36) Witters, D.; Knez, K.; Ceyssens, F.; Puers, R.; Lammertyn, J. *Lab Chip* **2013**, *13* (11), 2047−2054.
(37) Han, X.; Wang, R.; Zhou, Y.; Fei, L.; Sun, H.; Lai, S.; Saadatpour, A.; Zhou, Z.; Chen, H.; Ye, F.; et al. *Cell* **2018**, *172* (5), 1091−1107 e1017.
(38) Yuan, Z.; Wang, Z.; Guan, P.; Wu, X.; Chen, Y.-C. *Adv. Opt. Mater.* **2020**, *8* (7), No. 1901596.
(39) Zhou, Y.; Yuan, Z.; Gong, X.; Birowosuto, M. D.; Dang, C.; Chen, Y.-C. *Adv. Photonics* **2020**, *2* (06), No. 066002.
(40) Jana, S.; Xu, X.; Klymchenko, A.; Reisch, A.; Pons, T. *ACS Nano* **2021**, *15* (1), 1445−1453.
(41) Wang, Z.; Fang, G.; Gao, Z.; Liao, Y.; Gong, C.; Kim, M.; Chang, G.-E.; Feng, S.; Xu, T.; Liu, T.; Chen, Y.-C. *Nano Lett.* **2023**, *23* (7), 2502−2510.
(42) Fang, G.; Lu, H.; Law, A.; Gallego-Ortega, D.; Jin, D.; Lin, G. *Lab Chip* **2019**, *19* (24), 4093−4103.
(43) Fang, G.; Chen, Y.-C.; Lu, H.; Jin, D. *Adv. Funct. Mater.* **2023**, *33* (19), No. 2215043.
(44) Lu, H.; Stenzel, M. H. *Small* **2018**, *14* (13), No. 1702858.
(45) Jafarpour, S.; Ahmadi, S.; Mokarian, F.; Sharifi, M.; Ghobakhloo, S.; Yazdi, M.; Nedaeinia, R.; Salehi, R. *J. Drug Delivery Sci. Technol.* **2024**, *92*, No. 105375.
(46) Paskeh, M. D. A.; Entezari, M.; Mirzaei, S.; Zabolian, A.; Saleki, H.; Naghdi, M. J.; Sabet, S.; Khoshbakht, M. A.; Hashemi, M.; Hushmandi, K.; et al. *J. Hematol. Oncol.* **2022**, *15* (1), 83.
(47) Huang, B.-W.; Gao, J.-Q. *J. Controlled Release* **2018**, *270*, 246−259.
(48) Liu, Y.; Ma, L.; Hua, F.; Min, Z.; Zhan, Y.; Zhang, W.; Yao, J. *Oncogene* **2022**, *41* (14), 2012−2025.

https://doi.org/10.1021/acs.analchem.4c06172
Anal. Chem. 2025, 97, 5605−5611